Chapter 17

Identification of Fe_3O_4 Nanoparticles Biomedical Purpose by Magnetometric Methods

Zoia Duriagina, Roman Holyaka, Tetiana Tepla, Volodymyr Kulyk, Peter Arras and Elena Eyngorn

Additional information is available at the end of the chapter

http://dx.doi.org/10.5772/intechopen.69717

Abstract

The application of magnetic nanoparticles for biomedical research is an interdisciplinary problem. The use of nano- and microsized powder materials as developed technology for obtaining bionanomaterials with magnetocatalytic properties has been investigated. Control over immobilization can be carried by means of magnetic properties. Synthesis of superparamagnetic nanoparticles is developed not only for the benefit of fundamental science, but also for many technologies, such as technologies of magnetic storage media, magnetic ink for printers, but mainly for biosensors and medical applications. All the biomedical applications require that the nanoparticles have high enough levels of saturation of magnetization; their size should be less than 100 nm with a small deviation in size. Appropriate coating of the surface of magnetic nanoparticles should be nontoxic, biocompatible with the target of bioorganic compound. The techniques of measurement of magnetic nanoparticle properties by means of vibrational magnetometers, as well as by means of a set of smart sensor devices in accordance with new concept of Internet of Things (IoTh), were described. The first method is based on vibrating sample magnetometer technique. The second method is based on direct measurement of three dimensions (3D) of nanoparticles' magnetic field components.

Keywords: magnetic nanoparticles, drug transportation, magnetic field sensor

1. Introduction

Use of nanomaterials has become one of the innovation research directions in materials science, biochemistry and medicine. Small sizes of nanoparticles (NPs) lead to the appearance

of new unique functional properties. The methods of such material preparation are improving every year and become more accessible. The technology of material structure "design" by combining different types of materials, starting from metals, their compounds (oxides, nitrides, borides and hydrides) and ending with organic and inorganic polymers [1], has recently been widely used. Nanomaterials based on metals operate in power generating, optical industry and biomedicine. The unique superparamagnetic, optical and electrochemical properties are accentuated first of all. Use of magnetic nanoparticles (MNPs) for biomedical researches is an interdisciplinary problem and to solve it experts in different areas are required—medical workers, biologists, specialists in the field of materials science and electrodynamics. Application of nanomaterials with coating for biomedical purposes foresees such functional properties of the given system as adsorption, adhesion strength, biocompatibility, and certain magnetic and optoelectronic properties that will identify the stability of the obtained structure-energy state. The task of the materials science researchers is to develop complicated nanoobjects with optimal properties and morphological structure and to create the system of monitoring (Internet of Things (IoTh)) by their life activity cycle. The perfect biomedical systems can be considered such that the stable functional properties are possessed.

In particular, magnetism of nanoparticles is an important information carrier and what is especially valuable can be implemented through industrial means. This action at a distance in combination with a typical magnetic field penetration into human body tissues opens many new applications, including transport and purposeful delivery of biomagnets to a corresponding biological object [2]. Magnetism can be exhibited in a greater number of new nanomaterials. It is known that, under transition to nanosizes in metals and their compounds, new specific characteristics appear. Thus, magnetic properties of bulk gold and platinum are nonmagnetic, but at the nanosize they are magnetic. Surface atoms are not only different to bulk atoms, but they can also be modified by interaction with other chemical species, that is, by capping the nanoparticles. This phenomenon opens the possibility to modify the physical properties of the nanoparticles by capping them with appropriate molecules. Actually, it should be possible that nonferromagnetic bulk materials exhibit ferromagnetic-like behavior when prepared in a nanorange. One can obtain magnetic nanoparticles of Pd, Pt and the surprising case of Au (that is diamagnetic in bulk) from nonmagnetic bulk materials. In the case of Pt and Pd we can obtain the ferromagnetism. However, gold nanoparticles become ferromagnetic when they are capped with appropriate molecules: the charge localized at the particle surface gives rise to ferromagnetic-like behavior. This observation suggested that modification of the d band structure by chemical bonding can induce ferromagnetic-like character in metallic clusters [3].

2. Use of magnetic nanoparticles in medicine

Magnetic biomaterials are widely used in medicine, especially in cardiology, neurosurgery, oncology, radiology and cellular biology for cell separation, to perform immunological analysis, magnetic resonance spectroscopy, information preservation and so on [1–8]. They are also used as the X-ray contrast means and magnetosensitive composites for drugs and genes delivery, in radionuclide therapy and hyperthermia (**Figure 1**). Such applications are

http://dx.doi.org/10.5772/intechopen.69717

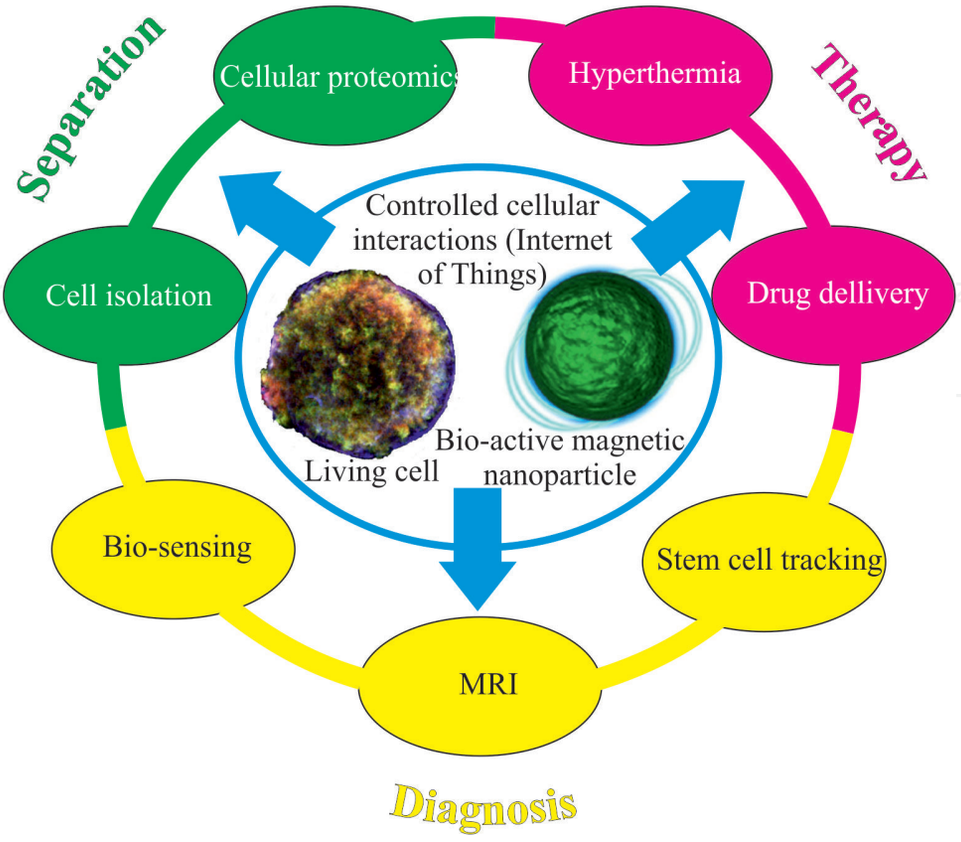

Figure 1. Use of magnetic nanoparticles in medicine.

perspective in case the clearly defined and checked interaction between magnetic nanoparticles and living cells is provided.

It is known that living organisms are built of cells with usual sizes of about 10 μm. The objects from which a cell consists of are much less than 1 μm. It should be considered that the synthesized nanoparticles are of sizes 2–450 nm, commensurable with the sizes of intercellular biological objects, viruses, proteins and genes. Thus, the nanoparticles by the sizes and mass occupy the intermediate place between single molecule and living cells. Still the main advantage of these materials is their ability to perform the preset functions under the effect of external magnetic field (**Figure 2**).

This occurs due to the formation of potential barriers at their boundary that limit the charge carrier movement in different directions and give the electron processes a mainly quantum character with dominating role of the interface. It should be noted that in this case a nonlinear dependence of equilibrium concentration of defects at the interface is observed that increases the dependence of properties on nanostructure sizes [10]. This is especially important when delivering drugs and means of diagnostics. Depending on the sizes, other properties of nanoparticles as toxicity, adsorption ability and magnetism also change. In particular, when the size of nanoparticles is less than 10 nm, they pass into a superparamagnetic state that, when adsorbing the energy of the external high-frequency electromagnetic field, promotes conversion of the energy state into the thermal one. This enables a tumor heating to a temperature of 43°C and thus its destruction [11, 12].

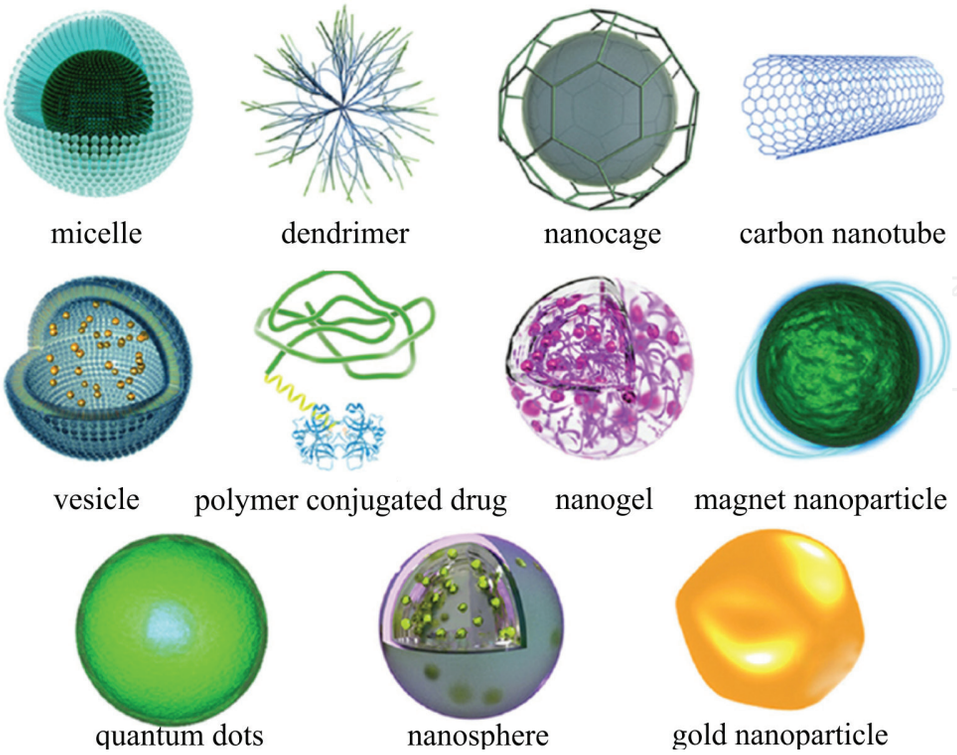

Figure 2. Several classes of NP used for the design of smart micro/nanocarriers, including micelles, dendrimers, nanocages, CNT, polymeric conjugates, nanogels, magnetic NP, quantum dots (QD), nanospheres and gold (Au) NP [9].

It has recently been proven that the effects of heat are more cytotoxic for cancer cells than they are for surrounding normal cells. Because of this, researchers have focused on hyperthermia as a method to selectively treat cancer cells. In Gilchrist's invaluable study, the cancer cells were heated locally using magnetic NP with a 1.2-MHz magnetic field. Since then, other observations have demonstrated that magnetic-induced hyperthermia in animals that have been injected directly with MNP can produce tumor regression through the application of magnetic fields to the solid tumors [9].

For therapeutic aims, magnetic nanoparticles are rarely used in a pure form. Usually, they are encapsulated or situated in bioinert matrices made of different organic compounds (**Figure 3**). This allows decreasing of the possible toxic effect of magnetic phase and simultaneous increasing of its stability due to immobilization on the surface of such capsules or matrices of medical aids. Encapsulation is usually carried out in suspensions of ultradispersive ferromagnetic or superparamagnetic particles containing stabilizing reagents—so called magnetic liquids [2, 5].

The structure of a multifunctional/multimodality MNP with a magnetic core, a polymeric coating and targeting ligands extended from the surface of MNP with the aid of polymeric spacers. Therapeutic payloads (drugs and genes) and imaging reporters (fluorophores and radionuclides) can be either embedded in the coating, or conjugated on the surface [5].

Magnetic contrast agents using which an image of a human body is obtained with a nuclear magnetic resonance tomography are widely known. Particles of these agents consist of a core

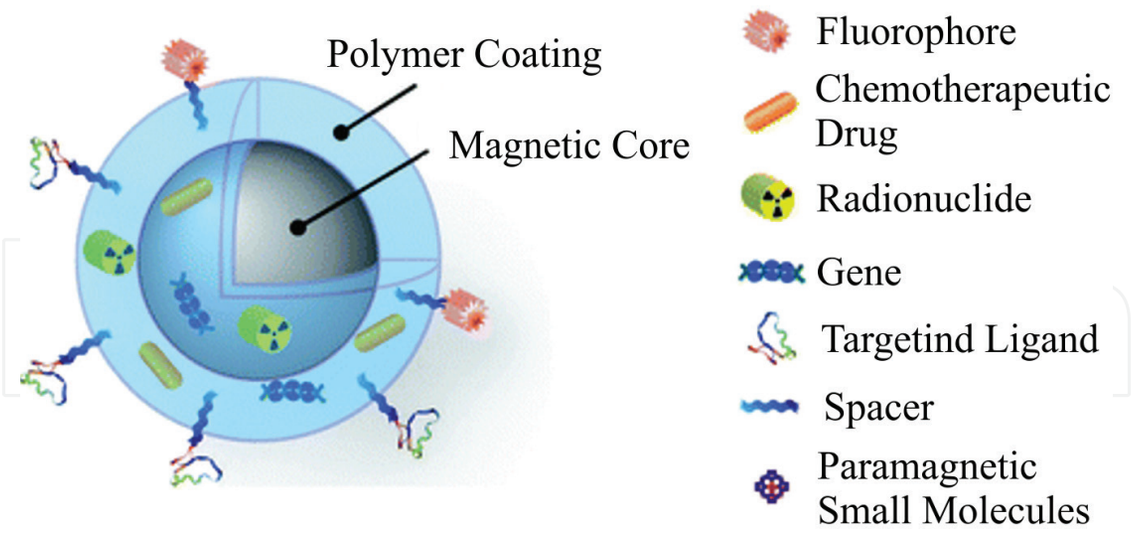

Figure 3. Graphic illustration of the structure of a multifunctional/multimodality MNP and different types of magnetic cores.

form magnetite or maghemite and a shell from dextran or silicon. Colloid solutions based on biomolecule-sorbed magnetic iron oxides, surrounded by a polymer layer, can be used for interaction with biological targets and direct them into a tumor with the aim of treatment or diagnostics. In this case, the controlled movement of magnetic particles in a body occurs because of the use of magnetic field gradient, regulated such that particles penetrate directly into the affected area [4].

Magnetic nanoparticle-based drugs can be divided into two groups: for external use (ointments, applicators, etc.) and for internal use (liquids, suspensions and magnetic containers). To improve physicochemical and medical biological properties when delivering drugs, the sizes of magnetic material particles in the blood stream should not exceed 100 nm. Under such conditions, they can be also used for hypoferritic anemia treatment. Today, the drugs obtained by adding precious metals to iron are paid more and more attention to. They are used as anti-inflammatory, antibacterial, anticancer and anesthetic compounds of the ointments for external use.

Magnetic carriers of medical purpose should be biocompatible with a human organism, nontoxic and nonallergenic. To improve biocompatibility, magnetic carriers are coated with chitosan, dextran, starch, carbon, gelatin, polymer starch coatings and so on (**Figure 4**). It should be noted that silicon oxide also increases biocompatibility of nanoparticles, and in this case, iron is localized inside the SiO_2 particles as in microcapsule. Release rate of drugs in these conditions can be regulated by changing the size and porosity of the obtained systems [4].

Recently, nano- and microsize powder materials are based on Fe_3O_4, especially in combination with bioselective elements—ferments have been widely used. This is important for developing technologies of manufacturing bionanomaterials with catalytic properties. High chemical activity of Fe_3O_4particles is caused by their higher ability to ion or atomic exchange, adsorption and formation of surface ligaments with other adsorbed particles. This guarantees

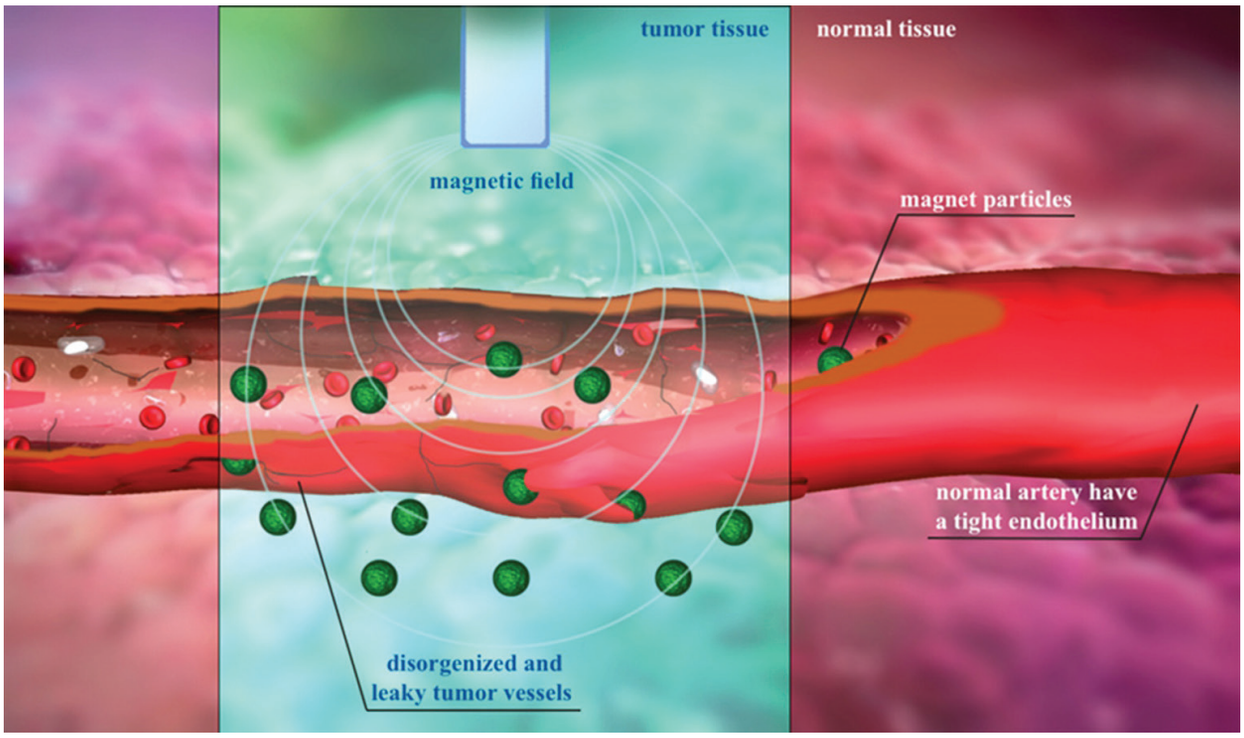

Figure 4. Schematic representation of the proposed magnetic sensitive carrier and triggered drug release mechanism [9].

the creation of bioparticles (immobilized ferments on the particle surface) with their further use in biosensorics and in enzymatic reactions. It is known that powder particles of Fe_3O_4 retain magnetization even if no external magnetic field is present, possessing own magnetic moment. However, remaining magnetization has a negative effect—a tendency of nanoparticles to agglomeration. Therefore, for the effective use of such magnetic particles, their chemical stability should be ensured by applying the corresponding coating on their surface.

2.1. Methods of obtaining magnetic nanoparticles

Physical and chemical properties of magnetic nanoparticles are determined by their structure and method of preparation. In most cases, these are particles of size from 1 to 100 nm with clearly expressed superparamagnetism. The most widely used methods of magnetic nanoparticle synthesis are as follows:

- Deposition—synthesis of iron oxides from water solutions of their salts in inert gas atmosphere at ambient or elevated temperature.
- Thermal decomposition—synthesis of Fe_3O_4 nanoparticles during decomposition of organic metal compounds in boiling organic solvents that contain stabilizing surface active agents (SAA).
- Microemulsion technology.

To synthesize magnetite-based nanocomposites, the following methodical approaches are mainly used [13–16].

- Precipitation in the conditions of oxidizing hydrolysis of iron sulfate Fe^{2+} in acid environment.
- Precipitation in the conditions of alkali hydrolysis of iron chlorides Fe^{2+} and Fe^{3+}.
- Precipitate deposition from the solutions of iron chlorides Fe^{2+} and Fe^{3+} under alkali hydrolysis of urea.

When modifying the conditions of magnetite core synthesis and forming the core shell, it is possible to obtain magnetic nanocomposites that differ not only by size but also by the ratio of "core–shell" sizes, magnetic susceptibility and complexity of surface microrelief that will specify the absorption properties.

However, nanoparticle synthesis has remained until now a complicated task. This is related with the difficulty of formation of homodispersive population of checked-size magnetic particles. It should be noted that there is no still a complete understanding of the mechanisms of core formation and growth. Besides the technology of obtaining crystalline nanoparticles with high saturation, magnetization needs further improvement. Moreover, nanoparticles lose their stability with time. This occurs due to the decrease of their free surface energy as a result of agglomeration. It is necessary to develop strategies of the surface coating preparation to simplify the process and effectively prevent agglomeration and segmentation of superparamagnetic particles. As a result, a stable solution for injections or frozen-dried (lyophilized) powder, that is easily dissolved, can be obtained [17].

Investigation of superparamagnetic nanoparticles, especially Fe_3O_4 nanoparticles, should be aimed at establishing the interrelations between their structure and pharmacokinetics. Nature of the coating on the iron oxide surface will determine not only the size of colloids but also will affect the pharmacokinetics and metabolic properties. This will enable modeling of their capture by reticuloendothelial system (RES) and facilitate diffusion to the tumor tissue. Processes of modification of magnetic nanoparticle surface, which are used for connection of biovectors, must be also improved. This is decisive in optimization of superparamagnetic nanoparticles likeness with biological objects [18].

2.2. Properties of Fe_3O_4 magnetite

Iron oxides (in particular magnetite) are among the most investigated materials in human history. Synthesis of superparamagnetic nanoparticles of iron oxide Fe_3O_4 is developing for the sake of fundamental science and technological applications, as for example magnetic data carriers, for biosensor, medical applications and magnetic inks [19–21]. Superparamagnetic nanoparticles of iron oxide with corresponding surface microgeometry can be used for increasing the image contrast, restoration of tissues, detoxification of biological fluids, hyperthermia, directed delivery of drugs and cell separation.

Detailed characterization of magnetite NPs is therefore necessary in order to obtain an accurate relationship between their electronic, magnetic and structural properties. Nominally claimed magnetite NPs are often (and to various extents) composed of nonstoichiometric oxide phases, and their instability in air ultimately causes oxidation to maghemite. The oxidization rate of

magnetite NPs in ambient conditions is size-dependent and can range from several months for NPs <10 nm, up to several years for NPs ~100 nm. However, there is no general consensus regarding the complex oxidation mechanism, which presumably proceeds through a continual set of intermediate phases accompanied by cations and vacancies (C–V) reordering. Magnetite and maghemite both crystallize in the face-centered cubic (fcc) spinel structure, whose unit cell is composed of 32 O^{2-} ions placed at the 32e crystallographic position, and 24 Fe ions distributed over the 64 tetrahedral 8a (A) and 32 octahedral 16d (B) crystallographic positions (**Figure 5**). Magnetite and maghemite can be represented with a single formula: $(Fe^{3+})_A[(Fe^{2+})_{1-3\delta}(Fe^{3+})_{1+2\delta\ \delta}]_B O^4$, where stands for vacancies and $0 \le \delta \le 1/3$. In pure magnetite ($\delta = 0$), all A sites are occupied by Fe^{3+} ions, while B sites are equally occupied with Fe^{2+} and Fe^{3+}. In pure maghemite ($\delta = 1/3$), all Fe ions are in 3+ state, with a tendency to regular arrangement

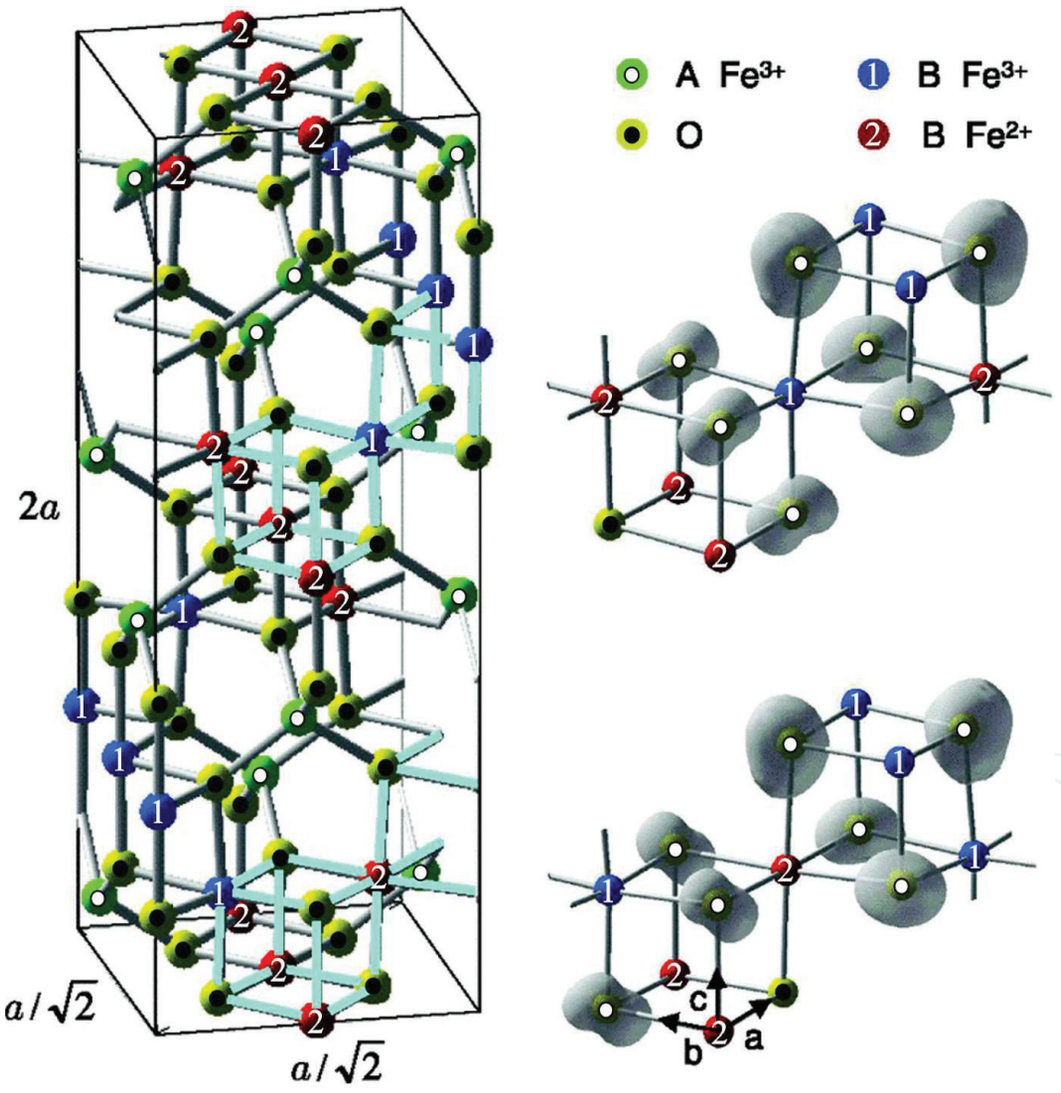

Figure 5. Left: monoclinic crystal structure of Fe_3O_4 in the low-temperature phase corresponding to a subcell of a2×a2×2a with P2/c symmetry. Right: 3D isosurfaces of unoccupied density of states of the O 2p integrated between the fermi level and 1 eV above within the corresponding Fe_3O_4 cubes highlighted in the crystal structure. For simplicity, we denote the octahedral Fe site with nominal 2+ and 3+ valences as Fe^{2+} and Fe^{3+}, respectively [22].

at B sites (two occupied followed by one vacant site). Vacancies occur preferentially at octahedral sites, but they can also mix over octahedral and tetrahedral sites. The degree of vacancy ordering in maghemite decreases with a particle size, and it is believed that for NPs smaller than 20 nm vacancy ordering vanishes. Magnetite and maghemite are both ferrimagnetic (the two uneven ferromagnetic sublattices Fe_A and Fe_B are antiferromagnetically aligned), with comparable saturation magnetizations (MS = 90 emu/g for magnetite; MS = 83.5 emu/g for well-ordered crystalline maghemite samples) and extraordinary high Curie temperatures (TC = 858 K magnetite; TC = 790–893 K maghemite, depending on the degree of C–V ordering).

The important difference between magnetite and maghemite is that maghemite is an insulator with energy gap Eg ≈ 2 eV, while magnetite is half-metal with much narrower Eg = 0.1–0.5 eV (depending on the sample quality). Furthermore, bulk magnetite undergoes so-called Verwey order-disorder phase transition to the insulating state at temperatures 120–125 K, accompanied with structural change from cubic to monoclinic lattice symmetry and various anomalies in the physical properties. The decisive influence on this complex transformation is ascribed to charge and orbital ordering involved in the three-site distortions. The exact structural parameters of the low temperature (LT) crystal structure, which is thought to have at least four inequivalent octahedral Fe sites, are extremely difficult to determine.

Things are even more elusive when the sample size is in the nanometer range. According to some recent reports for NPs with the mean size ~ 50 nm, the Verwey temperature (TV) shifts down to 20 K and it cannot be observed for smaller particles. The Verwey transition is weakly size-dependent in magnetite NPs larger than 20 nm, slightly suppressed in NPs smaller than 20 nm, and completely vanishes for NPs smaller than 6 nm. These inconsistencies are often ascribed to the fact that final properties of magnetite NPs strongly depend also on structural order [23].

2.3. Investigation of the structure and properties of Fe_3O_4 nanoparticles

In this research, the Fe_3O_4–NP characterization was performed by infrared Fourier spectroscopy using spectrophotometer Bruker Vertex 70 with attachment attenuated total reflectance (ATR). Powder samples were dried on the microscope slide surface and irradiated by a laser beam.

The intensive peak from Fe_3O_4-NP at 600 cm^{-1}, similarly to micro X-ray spectral analysis, indicated the presence of Fe-O bonds in Fe_3O_4–NP (**Figure 6**, **Table 1**). Peak intensity increases from the value of 1200 cm^{-1}, and in the range of 600–1200 cm^{-1} a significant background of the wave number area of the substances of glass on which the samples were dried is observed. In this range, only a signal from Si-O (for a wave number 1053 cm^{-1}) is clearly seen. The blind area should contain signals from C-O (for a wave number of about 1100 cm^{-1}) and signals of group Si–O–C (for a wave number of about 1108 cm^{-1}).

Obtained data can be used as an introductory information for processing monitoring of dynamics in situ of nanoparticle modification.

Size of Fe_3O_4 particles strongly affects its microstructure and properties. **Figure 7** presents a difference in microstructure of Fe_3O_4 micro- and nanoparticles.

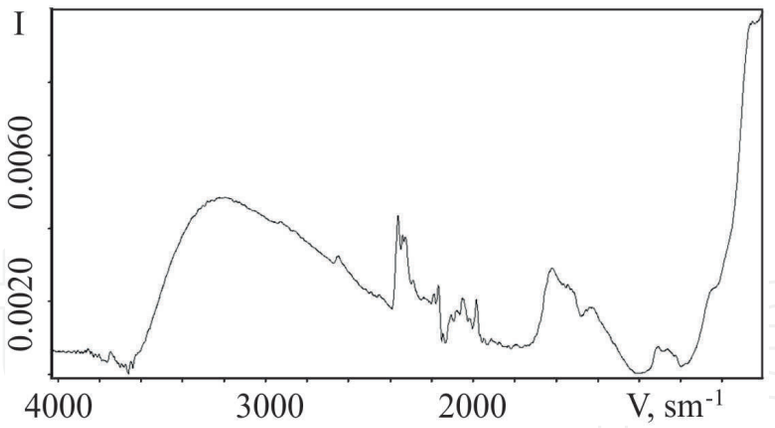

Figure 6. IR-Fourier spectra of Fe_3O_4 nanoparticles.

To estimate the sizes of Fe_3O_4-NP atomic-force microscopy was used, which software products allowed the establishment of the scanned particle structure (**Figure 8**). Investigation data prove the results of microscopic investigations on the spherical nanoparticle accumulation. Two types of structural inhomogeneity can be distinguished on the investigated sample surface: conglomerates of conical-like nanoparticles and granular texture of substrate. Surface topography is characterized by a rough relief with morphological regions of blocked structure. Blocks are characterized by nonisometric round form with no surface faceting. Their height above the substrate surface is in the range from 5 to 10 nm and base diameter from 30 to 50 nm. In this case, the dominant size of nanoparticles is 8 nm.

It is established at the same time that the size of Fe_3O_4microparticles is about 1μm (**Figure 9(b)**).

Use of Fe_3O_4nanoparticles with the aim of their functionalization (application of shells, medical aids and markers on them) or introduction in a living organism for hyperthermia foresees the application of surface coating. In this case, the analysis of the dimensions and properties of nanoparticles using a simple method becomes more complex [24]. In such cases, magnetic methods become one of the methods of particle categorization.

2.4. Methods of magnetic properties investigation

Among the magnetic research methods in materials science, the magnetic phase analysis is especially widely used. Its possibilities and effectiveness to a great extent are determined

Wave number (cm^{-1})	Chemical bond
3230	-OH valence vibrations
1617	-OH deformation (“wagging”)
1421	Not described
600	Fe-O

Table 1. Correspondence of IR-Fourier spectra peaks of Fe_3O_4–NP to chemical bonds [13–16].

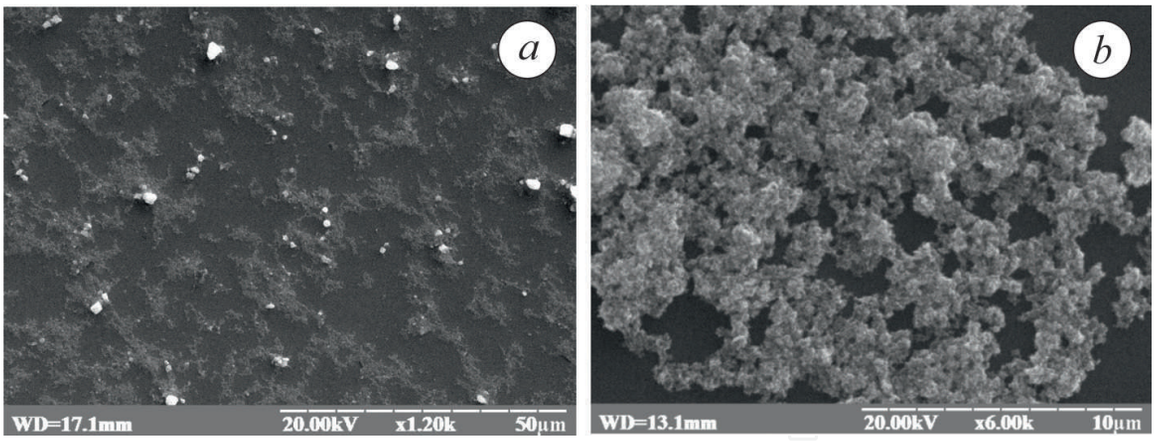

Figure 7. Microstructure of synthesized Fe_3O_4: (a) Fe_3O_4 nanoparticles; (b) Fe_3O_4 microparticles. Microstructures were obtained according to the scanning microscopy data.

by technical characteristics of the equipment. The quantitative phase magnetic analysis uses properties of ferromagnetics, which they acquire in strong magnetic fields—in the state of technical saturation. Primary magnetic properties that are structurally insensitive are obtained from the curve of temperature dependence of saturation magnetization. Such characteristics are magnetization and Curie point. These values give the information about phase composition of material and its changes in the process of certain thermal operations and also in the process of deformation. Curie point and saturation magnetization are called primary magnetic properties because their values are determined by the nature of the ferromagnetic phase (crystal lattice, electron structure of atoms and chemical phase composition) [25].

Changes in magnetization and Curie point of separate phases observed in the process of investigation of a certain material are not caused by their particle growth but are conditioned by the change of chemical composition of phases and their crystalline composition only. Based on these data, it is possible to study the kinetics of phase formation at the very early stages of the process (for particles sizes up to 10^{-6} cm) by the growth of magnetization and Curie point to their normal values. Thus, a weak dependence of saturation magnetization and Curie point

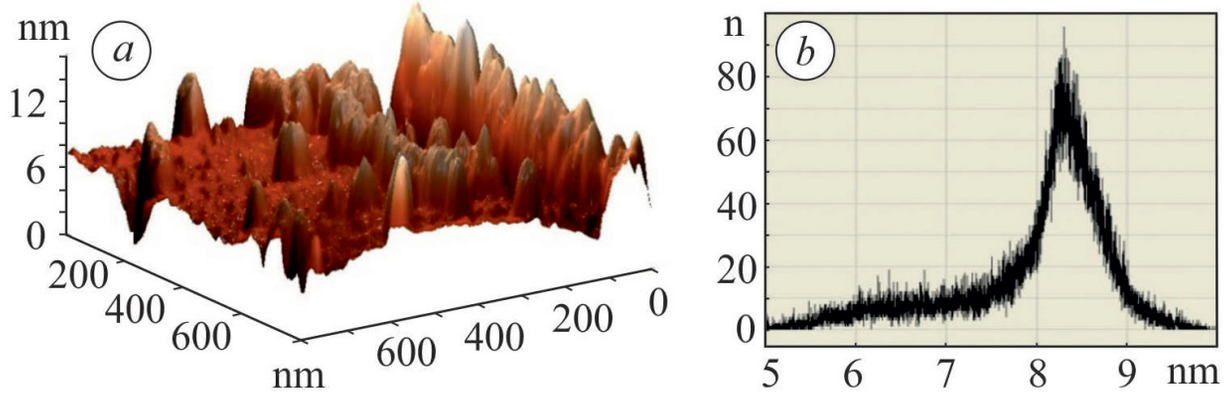

Figure 8. Character of distribution of synthesized Fe_3O_4-NP on the surface (a) and histogram of their distribution by size (b). Lateral dimension of particles in nanometers is given on X-axis, and a number of scanned particles on Y-axis.

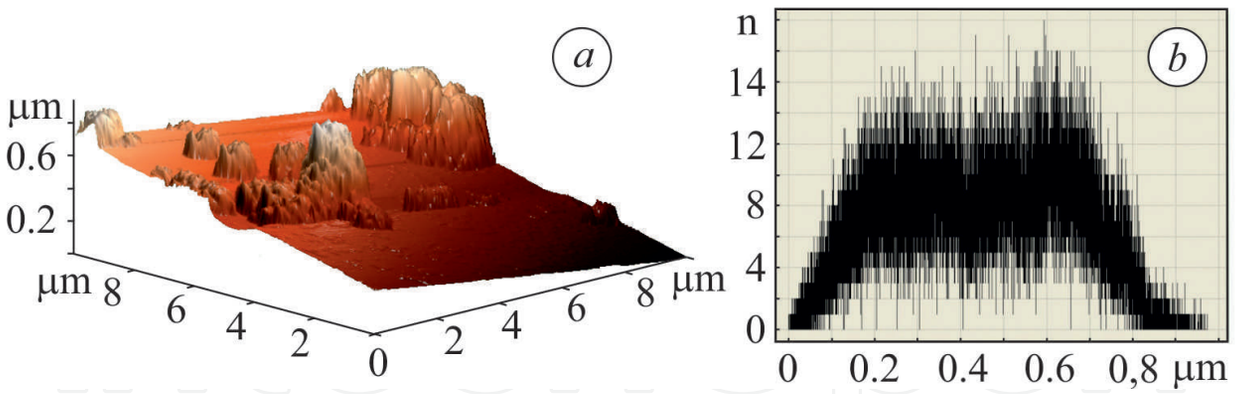

Figure 9. Character of distribution of synthesized microparticles of Fe_3O_4(a) and histogram of their distribution by size (b). Transverse dimension of particles in nanometers is given on X-axis, and a number of scanned particles on Y-axis (b).

on the stress state, form and degree of ferromagnetic dispersion allows us to choose these physical parameters as the quality characteristics of phases. Just these factors that strongly affect the results of the quantitative X-ray analysis, in the magnetic phase analysis, practically have no effect on the investigation results.

To carry out magnetic phase analysis, it is necessary to build experimentally a temperature dependence of saturation magnetization of the tested material sample. Equipment for the analysis should provide measuring of magnetic properties in a wide range of temperatures and heating and cooling rates. Peculiarity of the determination of the transition temperature of a number of dispersive magnetic systems to the paramagnetic state is that their magnetic phase analysis must be performed at high heating rates. Since in a number of cases the mass of the investigated samples can be very small (nanomaterials, fine-dispersive powders, amorphous films, surface layers after different types of heat treatment) and as a result the value of the magnetic moment is relatively small (from 10^{-2} to 10^{-3} А·м^2), the equipment must possess a very high sensitivity.

For such investigations, it is most reasonable to use the method of vibrating specimen that is realized through vibration magnetometers [26].

Measurement accuracy with vibration magnetometer depends on the calibration accuracy. We have proposed the method of comparison when magnetometer is calibrated using a standard with a known magnetic moment. As a standard, carbonyl iron of certain batches is used.

Application of the comparative method for calibration requires ensuring of the following conditions:

- insignificant changes in the position and deviation from the perfect sphere-like symmetry have no influence on a calibration constant;
- frequency and amplitude of vibrations remain constant;
- sample holder (container) introduces only an insignificant value to the signal value and can be subtracted from it; and
- signal voltage—linear function of the magnetic moment of the sample.

http://dx.doi.org/10.5772/intechopen.69717

Two measuring methods are used in vibration magnetometers—direct or compensation. The last one, in its turn, is of two types: the method of current shell and differential method. Compensation method allows avoiding the dependence of measuring results on the values of amplitude and frequency of vibrations. It is optimal to perform high-temperature measuring preliminary assuming the measures of stabilization of sample mechanical vibration. Constant amplitude and frequency of sample vibrations is a required condition of providing an adequate accuracy of measuring by the direct method.

The main cause of vibration amplitude instability is the changes in the moving parts of the magnetometer. Stability of measuring parameters is determined, in addition, by the stability of the alternating current generator which feeds the vibrator. Vibration amplitude stabilization was realized by providing a negative feedback of the generator.

Such a device for investigation of the magnetic properties possesses a number of unique characteristics. At room temperature, it is possible to build a hysteresis loop, partial hysteresis loops, initial curves of magnetization and demagnetization, and dependence of a magnetic moment on the sample orientation. At elevated temperatures, thermomagnetic measurements, high-temperature hysteresis measurements, and time dependences of magnetic moment at different temperatures can be carried out. Temperature measuring interval ranges from 80 to 1100 K at power 3.5 κWt. Magnetic measurement in this work was performed using a vibration magnetometer [15]. Curves of the investigated samples over magnetization were recorded in magnetic fields from −200 κA/m to +200 κA/m by measuring the dependence of the given magnetization I/I_{200}on the magnetic field strength H, I_{200}—magnetization at magnetic field strength 200 κA/m.

As one can see, curves of Fe_3O_4-NP sample remagnetization have a nonhysteresis form with a zero coercive force Hc and residual magnetization Ir (**Figure 10**(a)). Probably particles of Fe_3O_4 due to a high degree of dispersivity are in a superparamagnetic state—state that is typical of microscopic and nanoscopic particles of ferromagnetic materials. In this case, a magnetic moment of the like particle changes its orientation spontaneously and randomly or due to thermal fluctuations. When external magnetic field is absent, superparamagnetics

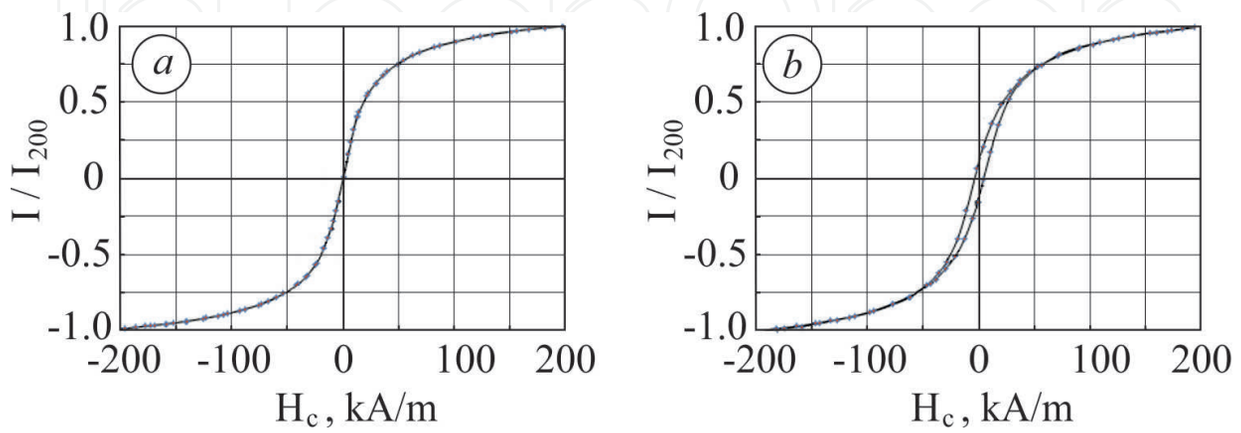

Figure 10. Curves of remagnetization of Fe_3O_4-NP (a) and Fe_3O_4-MP (b) samples.

have on average a zero magnetic moment, i.e., they behave like paramagnetics with a high magnetic susceptibility. As known, superparamagnetic properties of Fe_3O_4 particles at room temperature are exhibited, when reaching an average diameter D < 25 nm. In our case, the particles size is 5–10 nm.

With increasing sizes of Fe_3O_4 particles to microsizes, the magnetic properties do not change. These particles have already a hysteresis loop (**Figure 10(b)**). Samples' coercive force is H_c =4 κA/m, and ratio is I/I_{200}=0.1.

2.5. Use of the Internet of Things to measure of magnetic properties

For a remote study of magnetic properties of nanoparticles, it is proposed in this work to use the approaches of the Internet of Things—a network that consists of the interrelated physical objects or devices that contain mounted gauges. Their software allows one to pass and exchange data between physical world and computer systems using the conventional procedure of communication. In addition to gauges, the network contains executing devices, built-in physical objects interrelated by wire or wireless nets. These interrelated objects possess function of reading, putting in operation, programming and identification of objects and also allow one to exclude the necessity of person participation due to application of the intellectual interfaces.

Technology of magnetic particle detection and characterization is based on many approaches of magnetic sensing techniques [27, 28].

Here we present novel 3D magnetic sensors which offer three-dimensional sensing of orthogonal B_X, B_Y, and B_Z projections of magnetic field vector. Nowadays, many types of techniques and magnetic sensors provide such possibility [29, 30]. Among them, three types, namely magnetoresistors, Hall sensors and magnetotransistors, are preferable.

The first type, magnetoresistors, is based on the effect of magnetoresistance which is a tendency of material to change the value of its electrical resistance in an externally applied magnetic field. There are a variety of effects that can be called magnetoresistance: some occur in bulk nonmagnetic metals and semiconductors, such as geometrical magnetoresistance, Shubnikov de Haas oscillations, or the common positive magnetoresistance in metals. Other effects occur in magnetic metals, such as negative magnetoresistance in ferromagnets or anisotropic magnetoresistance (AMR). Finally, in multicomponent or multilayer systems (e.g., magnetic tunnel junctions), giant magnetoresistance, tunnel magnetoresistance and extraordinary magnetoresistance can be observed [31].

As an example, Honeywell International Inc. produced a series of magnetic sensors based on anisotropic magnetoresistance effect. AMR is a property of material in which the dependence of electrical resistance on the angle between the direction of electric current and the direction of magnetization is observed. AMR arises from the simultaneous action of magnetization and spin-orbit interaction, and its mechanism depends on the material. It can be for example due to a larger probability of s-d scattering of electrons in the direction of magnetization, which is controlled by the applied magnetic field.

AMR technology provides advantages over other magnetic sensor technologies. These anisotropic, directional sensors feature precision in-axis sensitivity, linearity, and low cross-axis sensitivity. For example, the HMC5883L is a small-size surface-mount, multi-chip module designed for low-field 3D magnetic sensing with a digital interface for applications such as low-cost compassing and magnetometry. The HMC5883L includes the state-of-the-art, high-resolution HMC118X series magnetoresistive sensors plus an application-specific integrated circuit, containing amplification, automatic degaussing strap drivers, offset cancellation and a 12-bit analog-to-digit converter.

The second type, Hall sensors, is based on Hall effect which is due to the nature of the current in a conductor. Current consists of the movement of many small charge carriers, typically electrons, holes or ions. When magnetic field is present, these charges experience a force, called the Lorentz force. When such a magnetic field is absent, the charges follow approximately straight "line of sight" paths between collisions with impurities, phonons and so on. However, when a magnetic field with a perpendicular component is applied, their paths between collisions are curved so that moving charges accumulate on one face of the material. This leaves equal and opposite charges exposed on the other face where there is a scarcity of mobile charges. The result is an asymmetric distribution of charge density across the Hall element, arising from the force that is perpendicular to both the "line of sight" path and the applied magnetic field. The separation of charge establishes an electric field that opposes the migration of further charge, so a steady electrical potential is established for as long as the charge is flowing.

We have proposed new type of thin-film magnetic field sensors for three-dimensional sensing of orthogonal B_X, B_Y and B_Z projection of magnetic field vector [32–37], new method for measuring magnetic field [38] as well as their modeling and signal processing [39–44].

The general view of such thin-film 3D sensors, its active area, structure and photographs are presented in **Figures 11–13**, correspondingly. The sensor (**Figure 12(a)**) active area is the thin sensitive semiconductor film (2) of corresponding configuration formed at the semi-insulating GaAs substrate (1). Sensor contacts are formed by the metallization layer (3), which typically is the gold film together with other metals, for example, with titanium sublayer. For manufacturing of the structures, three photolithographies are used. The first one is intended

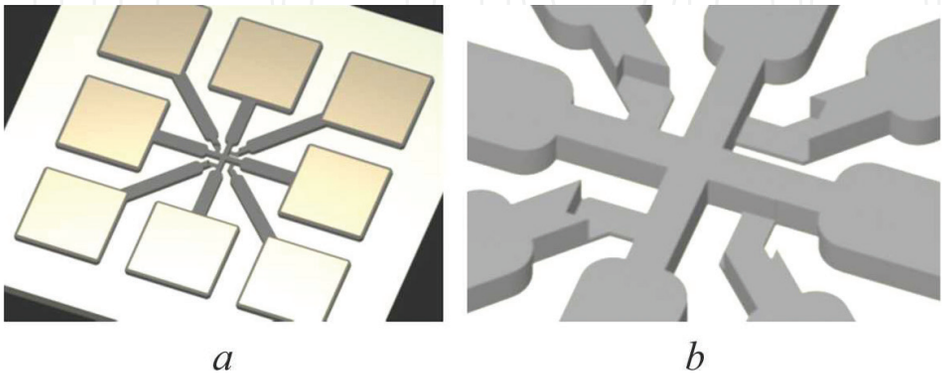

Figure 11. General view of thin film 3D sensors (a) and its active area (b).

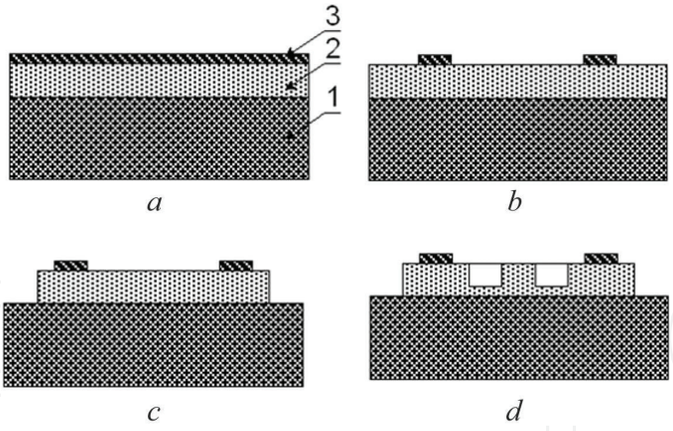

Figure 12. Structure and its formation stages (a), (b), (c), (d) of 3D thin film sensor: 1—substrate, 2—semiconductor active area; 3—contact metallization layer.

for creation of the contact system (**Figure 12(b)**); the second one is for etching a semiconductor film into the whole depth (**Figure 12(c)**); and the third one is for etching the semiconductor film to approximately 10% of their thickness (**Figure 12(d)**).

To show how a 3D thin-film sensor works, let us consider its main component—transducer #1 (**Figure 14**). The magnetic field vector projections B_X, B_Y are located in the transducer plane, and B_Z projection is perpendicular to this plane.

The operation principle of transducer of type #1 is the following: transducer is connected to the power source, typically direct current source; for this, the central current contact 3 is connected to the first power supply output, and side current outputs 4, 5 are connected together to the second power supply output. Thus, the current in the active area of the transducer is divided equally and run in mutually antithetical directions in relation to the current output.

Neglecting the current in the 6 and 7 voltage contacts' circuit, one may consider that the voltages at those outputs are equal to the corresponding voltages of the intermediate areas 10 and

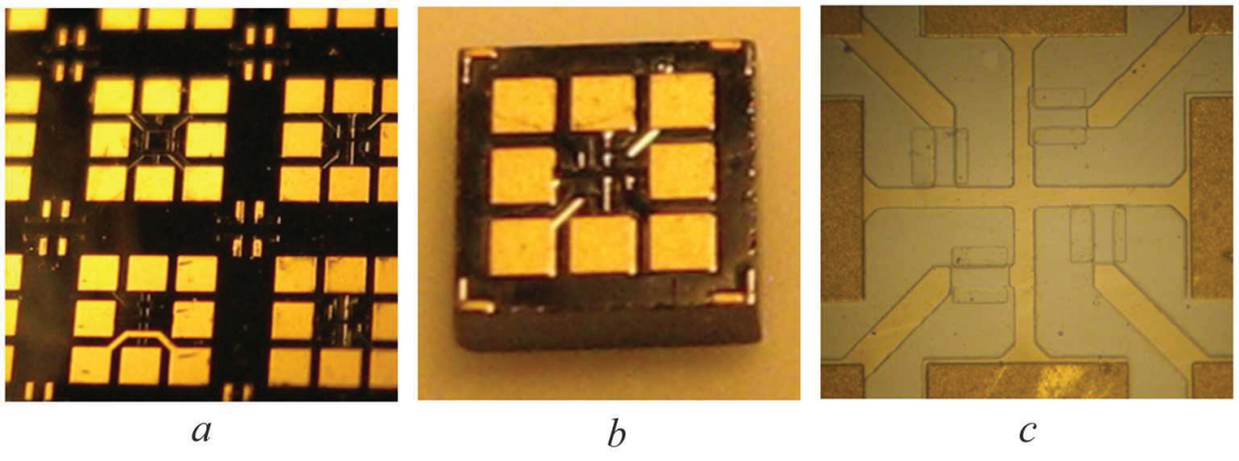

Figure 13. Photos of 3D thin-film sensors: wafer (a), chip (b) and active area (c).

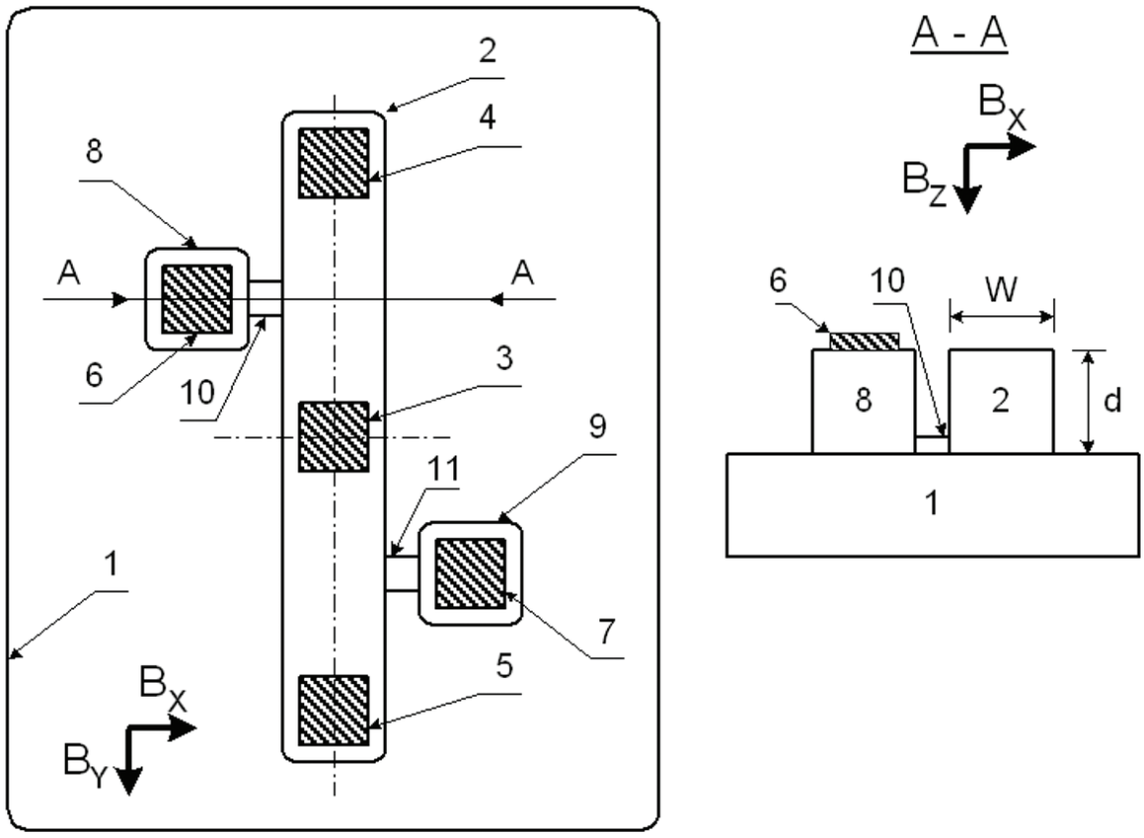

Figure 14. Structure of type #1 transducer: 1—substrate, 2—semiconductor active area; 3—central current contact; 4, 5—side current contacts; 6, 7—voltage contacts; 8, 9—auxiliary areas; 10, 11—intermediate areas.

11. So the construction of the type #1 transducer provides the possibility of forming the output voltage at the 6 and 7 voltage contacts, which is equal to the voltage difference between the areas of lower surface of the active area in the neighborhood for the contacting to the intermediate areas 10 and 11. The voltage measurement at the areas of lower active area surface is obvious that the thickness of intermediate areas 10, 11 was considerably thinner (at least 10 times) than the thickness of active area 2.

The principal difference of the type #1 transducer from analogs, for example Refs. [29, 30], is that in the first one the voltage difference is measured between the areas of lower active area surface, and in the analogs—between the areas of the upper active area surface. In its turn, the absence of contacts with the upper active area surface makes it possible not to perform the active area surface insulation.

In general case, the voltages at the voltage outputs 6, 7 are composed of three components. The first component V_R is caused by the voltage drop at the semiconductor active area 2. Taking into consideration the symmetry of the active area in relation to the first current contact 3, the first voltage component at both voltage contacts 6, 7 is equal $V_R(6) = V_R(7)$. The second component V_Z is caused by the influence of B_Z magnetic field vector projection, which is perpendicular to the transducer plane. Taking into consideration the transducer construction and current flow directions in it, the second voltage component at the voltage contacts 6 and 7 is also equal $V_Z(6) = V_Z(7)$. The third component V_X is caused by the influence of B_X projection

of induction vector. Contrary to the two stated above, this component at the voltage contacts 6 and 7 has the opposite signs $V_X(6) = -V_X(7)$. In particular, in the upper part of active area, two charge carriers under the influence of electromotive force deviated to the upper semiconductor layer surface, and then, in the lower part—to the lower surface (in the direction of substrate). The voltage difference caused by this carrier deviation is transferred to the voltage contacts 6 and 7 through the intermediate areas 10 and 11. It is to be noted that the B_Y magnetic field induction vector projection, parallel to the direction of current flow through the active area, does not cause the carrier deviation, and therefore, it may be neglected: $V_Y(6) = V_Y(7) = 0$.

Thus, the voltage difference between the voltage outputs 6 and 7 (output voltage of type#1 transducer) is determined only by B_X magnetic field induction vector projection, and in first approximation, it does not depend on other vector projections:

$$V_{OUT} = \left[V_R(6) + V_X(6) + V_Y(6) + V_Z(6)\right] - \left[V_R(7) + V_X(7) + V_Y(7) + V_Z(7)\right] = V_X, \quad (1)$$

where $V_X = V_X(6)+V_X(7)$.

The especially high efficiency of transducer of type#1 application is realized in case of their application in 3D sensor for simultaneous measurement of three projections B_X, B_Y and B_Z of the magnetic field induction vector. Such 3D sensor contains three coupled transducers at a single substrate. The construction of two transducers of #1 type is similar to **Figure 14**. They are mutually orthogonally rotated and provide the sensitivity to the BX, BY vector projections of the field induction vector. The third transducer, which provides the sensitivity to the BZ projection, is a traditional Hall transducer [29].

To provide the equal sensitivity levels for all three transducers of such 3D sensor, it is necessary to take into account the following: contrary to the traditional Hall transducers, which have the sensitivity as an inverse function of semiconductor active layer thickness d, the sensitivity of the transducer of type #1 is inversely proportional function of the semiconductor area width W. So it is recommended that the active area width W should be minimal and approximately equal to the semiconductor layer thickness d.

There are two other options to build up 3D magnetic thin film sensors. They are based on type #2 and type #3 transducers.

The structure of type #2 transducer is shown in **Figure 15**.

The type #2 transducer is fed by the direct current source, and one pair of mutually opposed current contacts (e.g., 3 and 5) is connected to one output of the power source (e.g., positive), and another pair (4 and 6 correspondently) to the other power source contact (negative, correspondently). In accordance with this connection scheme, the four current flow circuits are formed: I_{34}, I_{36}, I_{54} and I_{56}, where the indices in the marked currents correspond to the numbers of current contacts. These current flow circuits geometrically form the square sides. The matter of principal importance is that the currents that flow in opposed square sides are equal by value and opposed by sign: $\vec{I}_{34} = -\vec{I}_{65}$; $\vec{I}_{36} = -\vec{I}_{45}$. The output signal of transducer is the voltage difference between the voltage contacts. The informative signals about the magnetic field vector projections B_X, B_Y, B_Z are the voltages V_X, V_Y, V_Z, which in first approximation are determined as:

$$V_X = V_8 - V_{10};\ V_Y = V_7 - V_9;\ V_Z = \left\{(V_8 - V_9) + (V_{10} - V_7)\right\}/2 \quad (2)$$

The difference of type #2 transducer from its analog [29, 30] is the limitation of the area of current transition between the 2nd outer and 11 inner insulating areas. This provides the increase of the sensor sensitivity to the B_X, B_Y magnetic fields and decreases the cross-impact between the informative signals.

The sensitivity increase is explained by the reduction of the transducer active area size. Contrary to the traditional Hall transducers (sensitive to the field B_Z perpendicular to the transducer plane), where the size that determines the sensitivity is the active area thickness, in case of the B_X, B_Y field transducers, the determinative size is the current scattering region. The smaller area occupies the current scattering region, the higher is the voltage difference between the two corresponding voltage contacts, and therefore the higher sensitivity is.

The structure of type #3 transducer is shown in **Figure 16**.

Arms 2, 4 and contacts 6, 8, 10, 12 form the first vertical Hall transducer, and arms 3, 5 and contacts 7, 9, 11, 13—the second vertical Hall transducer. The first transducer is intended for measuring the B_X magnetic field vector projection, and the second one—for measurement of B_Y projection. The measurement principle of Hall transducers consists in forming the voltage difference at the voltage outputs during the deviation of charge carriers in the semiconductor area under the electromotive force influence.

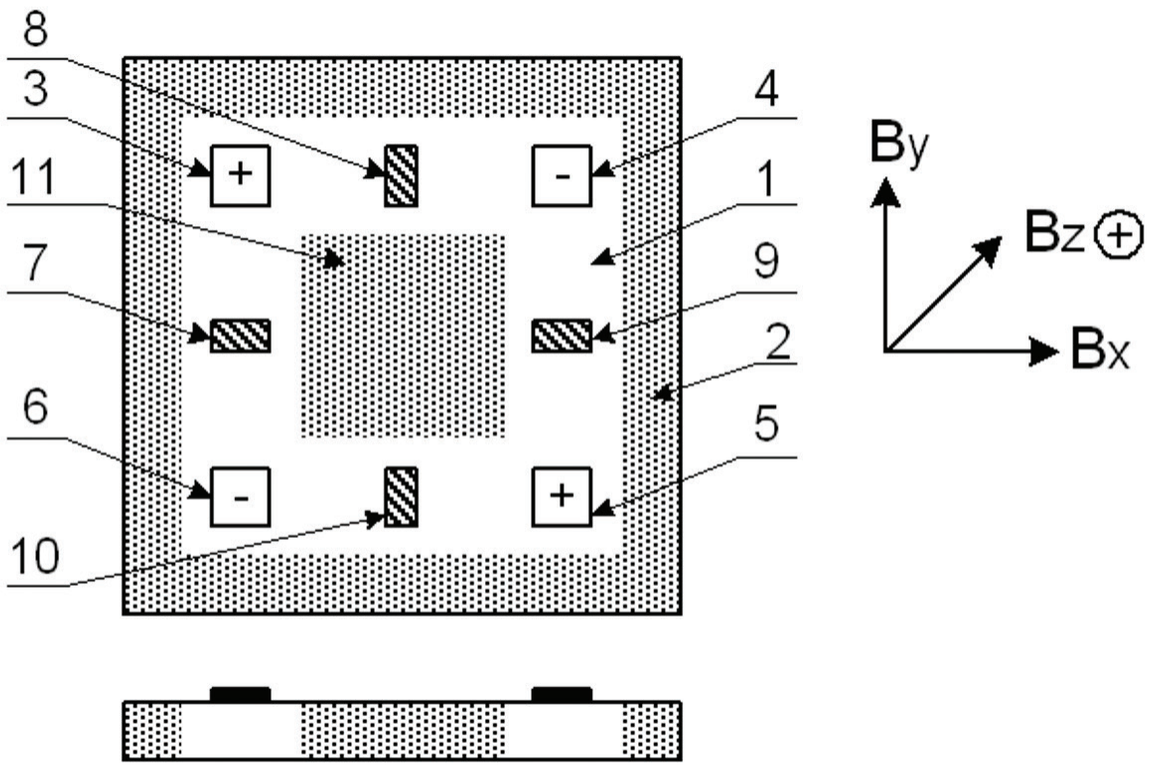

Figure 15. Structure of type #2 transducer: 1—semiconductor active area; 2—outer insulating area; 3, 4, 5, 6—current contacts; 7, 8, 9, 10—voltage contacts; and 11—inner insulating area.

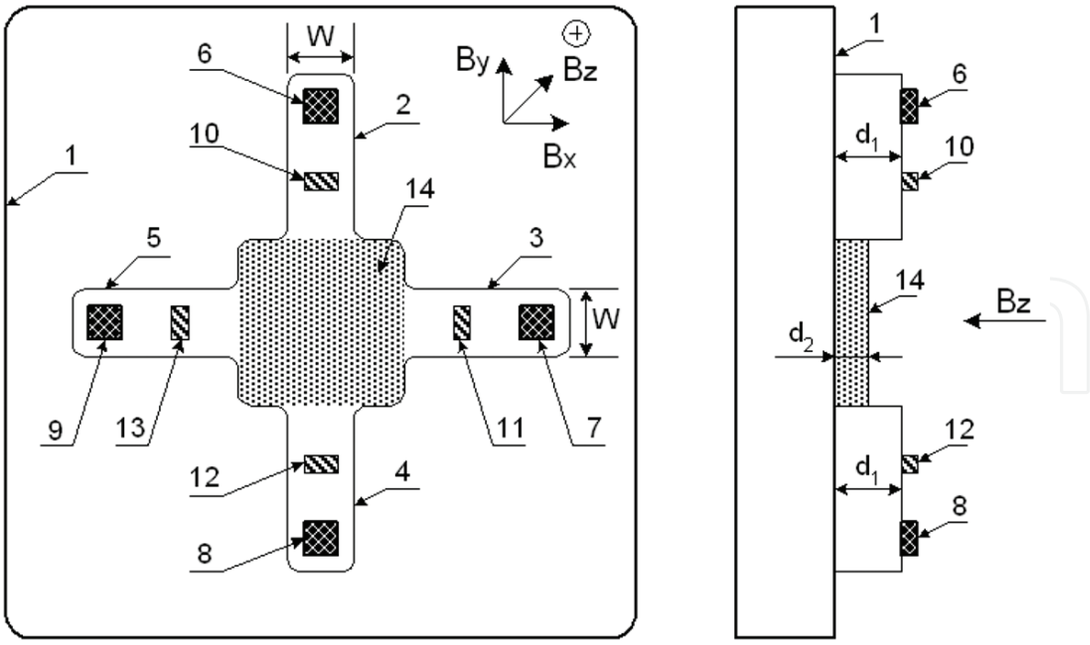

Figure 16. Structure of type #3 transducer: 1—substrate; 2, 3, 4, 5—four arms of cross-shaped figure, formed by the crossing of two semiconductor areas of vertical Hall transducers; 6, 7, 8, 9—current contacts; 10, 11, 12, 13—voltage contacts; and 14—semiconductor area of horizontal Hall transducer.

The operation of type #3 transducer presumes two power supplying modes. The first one provides the operation of the vertical Hall transducers, and the second one for operation of the horizontal one.

The first power-supplying mode presumes the connecting of the current contacts of the vertical Hall transducers, when the currents in their semiconductor areas are flowing in mutually opposed directions. For this, the current contacts of both vertical Hall transducers are connected into one circuit. Namely, contacts 6 and 8 of the first vertical Hall transducer are connected together and to the first, for example, positive output of the power source, and contacts 7 and 9 of the second vertical Hall transducer are also connected together to the second, therefore, negative output of the power source. So, in the first vertical Hall transducer, the currents are flowing from the top to the bottom (current I_2 in arm 2) and from the bottom to the top (current I_4 in arm 4), and in the second—from left to right (current I_3in arm 3) and from right to left (current I_5 in arm 5). In case of ideal symmetry of the transducer structure, the following equality takes place: $\vec{I} = -\vec{I}; \vec{I} = -\vec{I}$.

Output signals of vertical Hall transducers are formed at the voltage outputs as a voltage difference, which is proportional to the multiplication of the power supply current value of the transducer by the corresponding magnetic field vector projection:

$$V_X = V(12) - V(10) = K_X \times I \times B_X / W\text{–for the first transducer and} \quad (3)$$

and

$$V_X = V(12) - V(10) = K_X \times I \times B_X / W\text{–for the second transducer and} \quad (4)$$

where V(11), V(12), V(13) and V(14) are the voltages at the voltage outputs 11, 12, 13 and 14, correspondingly; V_X, V_Y and K_X and K_Y—output signals and transducing coefficients of the first and second transducers, correspondingly; I—operational current, W—the width of semiconductor areas.

From the physical point of view, the appearance of voltage difference at the voltage contacts of the vertical Hall transducers is explained by the fact that due to the opposed current flow directions in both transducer arms, the deviation of current carriers in those arms has also the opposed direction. In particular, in arm 2 of the first transducer, the carriers are deviated in the direction away from the substrate to the surface of the semiconductor area, and then, in arm 4 of this transducer—in the direction from the surface to the substrate.

In a high-gradient magnetic field, the voltage difference formed at the voltage outputs of the vertical Hall transducers is the informative value of the averaged field induction value. Taking into the consideration that all the voltage outputs of the vertical Hall transducers are equidistant from its center (crossing area), the measured averaged induction value corresponds to the spatial point of the transducer center.

The second power-supplying mode presumes the application of only one pair of current contacts, namely 6 and 8 of the first vertical transducer. Then, output 6 is connected to the first power supply output, and output 8 to the second one. This provides the linear trajectory of the charge carriers in semiconductor area 14 of the horizontal Hall transducer.

The output signal of the horizontal Hall transducer, as a voltage difference, is proportional to the multiplication of the transducer power supply current by the B_Z projection of the magnetic field induction vector, formed at the voltage outputs 11 and 13 of the second vertical Hall transducer: $V_Z = V(13)–V(11) = K_Z.I.B_Z/d_2$, where K_Z is the coefficient of transduction and d_2 is the thickness of semiconductor area of the horizontal Hall transducer.

From the physical point of view, the appearance of the voltage difference at the voltage outputs 11 and 13 is explained by the fact that charge carrier deviation in semiconductor area 14 of the horizontal Hall transducer under the influence of B_Z magnetic field induction vector projection is in the direction from arm 5 to arm 3, or backwards.

As in the vertical transducer, the horizontal Hall transducer measures the value of the magnetic field induction value in the transducer center spatial point. Thus, type #3 transducer allows measuring of all three projections B_X, B_Y and B_Z of the magnetic field induction vector in a single spatial point.

The other distinctive feature of the type #3 transducer is the possibility to change the d_2 thickness of the horizontal Hall transducer semiconductor area. This allows the formation of the transducer with equal sensitivity value to all three magnetic field induction vector projections: $V_X/B_X = V_Y/B_Y = V_Z/B_Z$. Taking into consideration that the sensitivity of vertical Hall transducers is inversely proportional to the semiconductor area width W, and for horizontal transducer—to the thickness of its semiconductor area d_2, the equality of the stated values of sensitivity is provided by the correspondent selection of W/d_2 ratio. It is important that contrary to the d_1 thickness of the vertical Hall transducer areas, the d_2 thickness of the horizontal transducer semiconductor area may change after the output formation. In particular, the decrease of d_2 thickness may be realized by partial etching of the semiconductor layer.

In relation to the analogs [29], the type #3 transducer provides the increase of the measurement accuracy and construction simplification.

The increasing accuracy is caused by the fact that horizontal Hall transducer is placed in the center (crossing area) of vertical Hall transducer. This provides the high spatial alignment of all transducers (two vertical and one horizontal), and therefore, all the three projections B_X, B_Y and B_Z of the magnetic field induction vector are measured at a single spatial point. During the measurement of high-gradient fields, this gives the ability to decrease the magnetic field induction vector measurement error in several times.

The third type, magnetoresistors, is mostly bipolar or field-effect transistors whose structures and operating conditions are optimized with respect to the magnetic sensitivity of its output currents. There are three major effects of magnetotransistors, namely the current deflection effect, the injection modulation and the magnetodiode effect.

We have proposed the structure of magnetotransistors adapted to three dimensional sensing of orthogonal B_X, B_Y and B_Z projections of the magnetic field vector (**Figures 17–19**). These are drift-aided lateral double-collector p-n-p transistors. The emitter area E and two collector p-type areas C1, C2 are embedded into plate-like n-type base region. The two base contact n^+ type areas B1, B2 are used to apply the bias voltage needed to establish the lateral accelerating electric field in the region. The emitter injects holes into the base region. Under the influence of the accelerating field in the base, these holes form a minority carrier beam. In the presence of normal B_Z magnetic field (**Figure 17**), the electric field in the base region rotates for the Hall angle of majority carries, and the hole beam tilts with respect to the electric field for the Hall

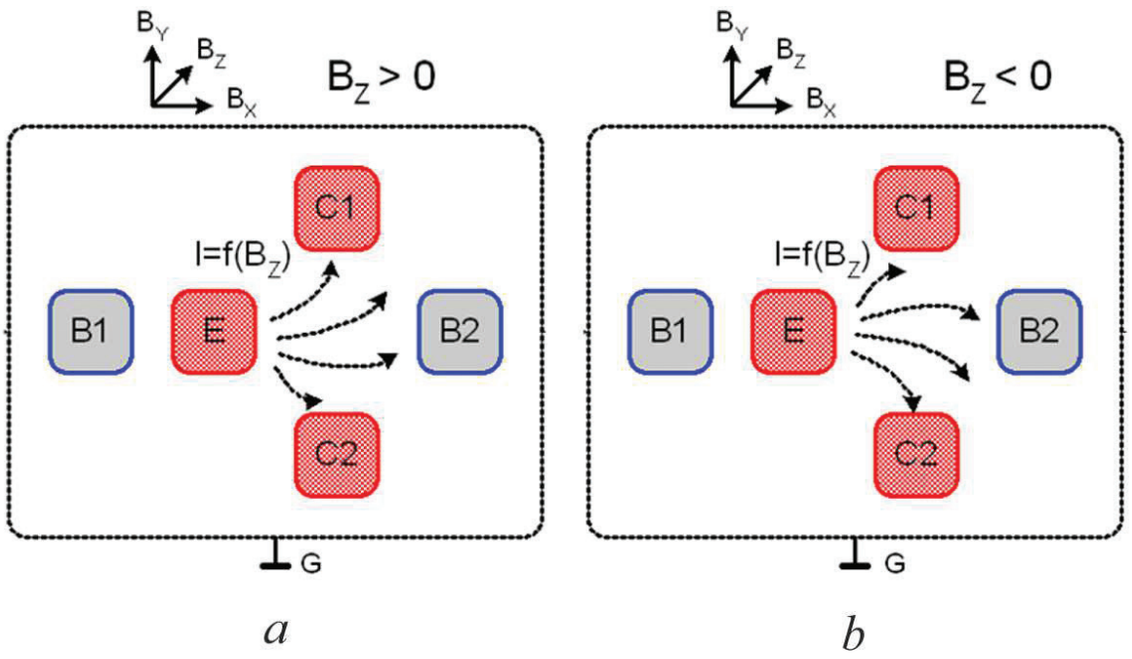

Figure 17. Structure of magnetotransistor (a) and current deflection (b) $I = f(B_Z)$ under B_Z magnetic field vector projection: B1, B2—base contacts; E—emitter area; C1, C2—collector areas; and G–connected to ground a p-n junction wall insulation.

http://dx.doi.org/10.5772/intechopen.69717

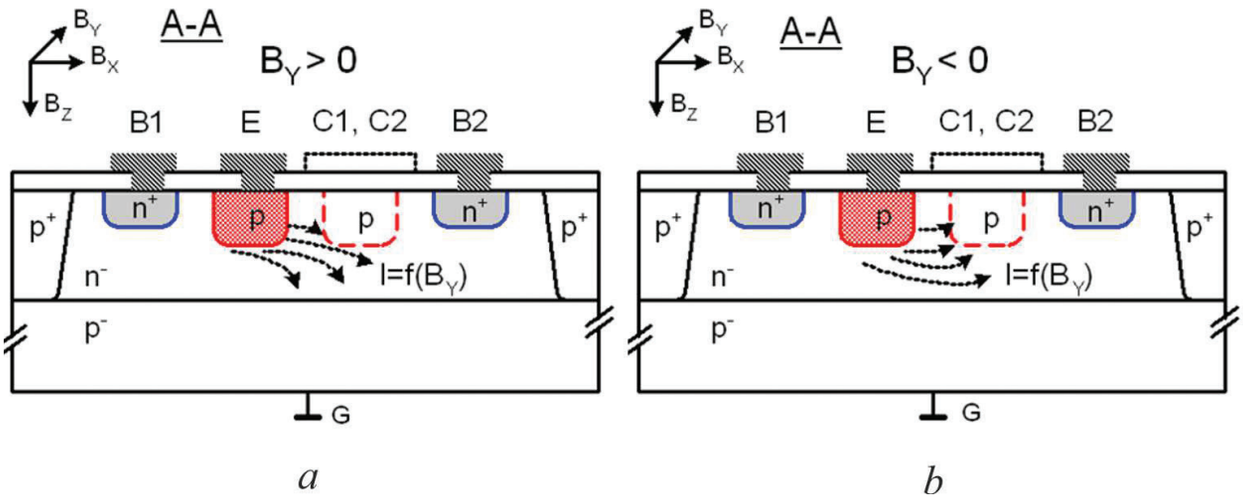

Figure 18. Structure of magnetotransistor (a) and current deflection (b) $I = f(B_Z)$ under B_Z magnetic field vector projection: B1, B2 (n^+ type)—base contacts; E (p type)—emitter area; C1, C2 (p type)—collector areas; G—a substrate connected to ground (p^- type).

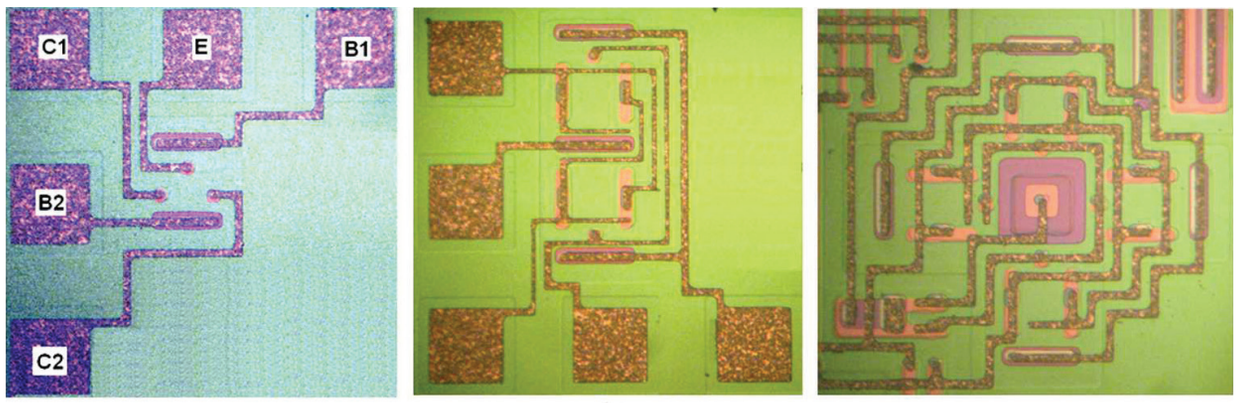

Figure 19. Photos of magnetotransistors: single (a), doubled (b) and quad (c) structures.

angle. The deflection of a beam leads to an imbalance in the two C1, C2 collector currents. In the presence of B_Y magnetic field vector projection (**Figure 18**), the hole beam tilts up to collectors or down toward a p^- type substrate connected to ground. Doubled and quad (**Figure 19**) structures are used to provide a set of signals in correspondence with three projections of magnetic field vector.

Based on the sensors proposed and described above, a set of magnetometers for detection and characterization of magnetic particles has been developed. For illustration only, an example of software windows for control and measurement result visualization, as well as a measurement resolution archived (in this case about 10^{-7}T), are shown in **Figures 20** and **21**. As it was noted, the main advantage of such sensors is a possibility of measuring three orthogonal projections of a magnetic field vector that is quite new in characterization of magnetic particle technique.

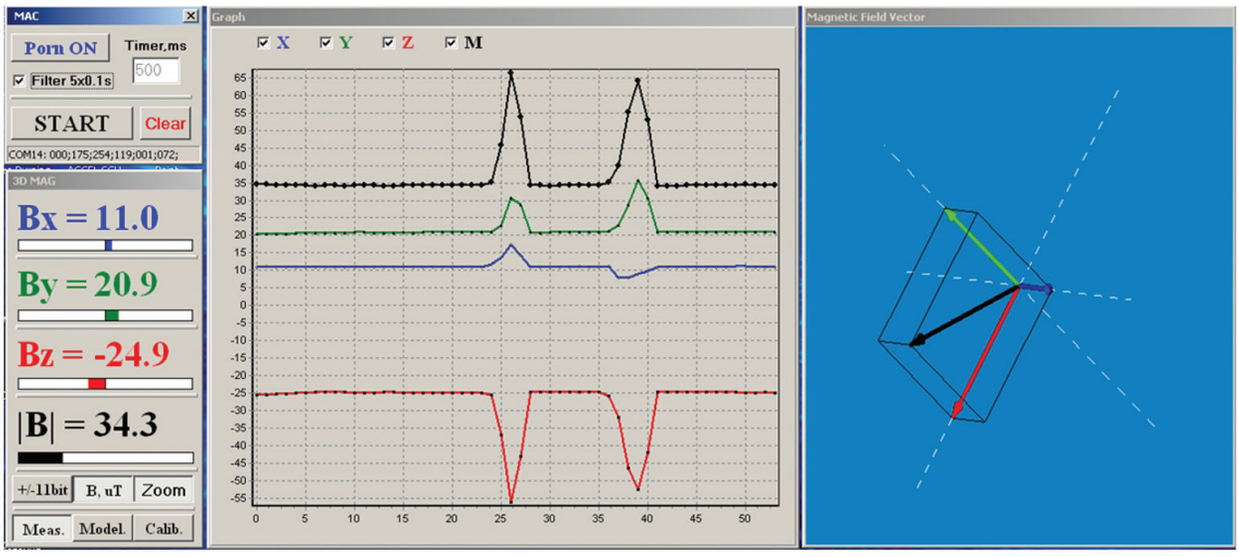

Figure 20. Software of magnetometer based on 3D sensors.

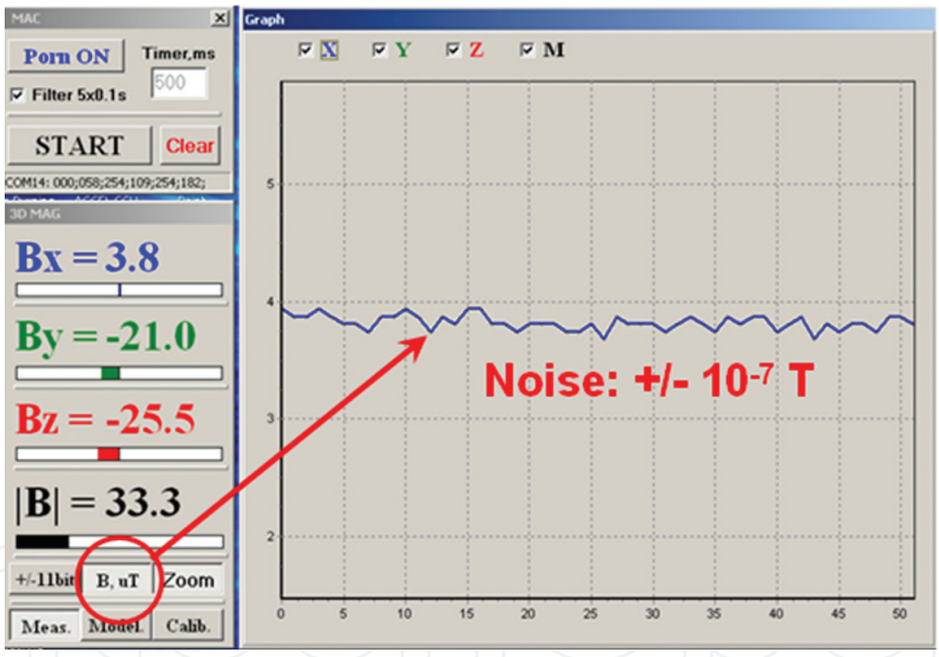

Figure 21. Measurement resolution (noise) of magnetometer based on 3D sensors.

3. Conclusion

It is possible to say that the interest to nanomaterials with magnetic properties increases every year. These materials have found their applications in medicine for diagnostics and treatment of serious diseases, where treatment by other methods is more expensive and durable. However, synthesis of such nanomaterials with stable properties is not completely elaborated, since besides the size factor, the character of their building microgeometry, functional

properties and methods of identification should be considered. Special attention should be paid to sizes, topography and biocompatibility of initial nanoparticles. Just these parameters finally determine the functional properties.

It is shown in the paper that identification of synthesized nanoparticles can be realized most effectively by the change of their magnetic properties. This is possible both at the stage of their synthesis and after biofunctionalization. Success of the proposed approach formed the basis of the ideology of the Internet of Things use for monitoring the stability of nanoparticles microstructure and their functional properties in application in medicine.

Acknowledgements

We are infinitely grateful to Mykhailo Gonchar and Tetiana Prokopiv from the Institute of Cell Biology of the National Academy of Sciences of Ukraine, Department of Analytical Biotechnology, for kindly provided samples of Fe3O4 powders for our research. Also we would like to acknowledge financial support of the Ministry of Education and Science of Ukriaine under Grant 0116U004142 and partially by funds of 543994-TEMPUS-1-2013-1-BE-TEMPUS-JPCR MMATENG (Modernization of two cycles (MA, BA) of competence-based curricula in Material Engineering according to the best experience of Bologna Process – EU).

Author details

Zoia Duriagina[1]*, Roman Holyaka[1], Tetiana Tepla[1], Volodymyr Kulyk[1], Peter Arras[2] and Elena Eyngorn[3]

*Address all correspondence to: zduriagina@ukr.net

1 Lviv Polytechnic National University, Lviv, Ukraine

2 KU Leuven, Sint-Katelijne-Waver, Belgium

3 Technische Universität Berlin, Berlin, Germany

References

[1] De Crozals G, Bonnet R, Farre C, Chaix C. Nanoparticles with multiple properties for biomedical applications: A strategic guide. Nano Today. 2016;**11**(4):435-463

[2] Nikiforov VN. Biomedical applications of magnetic nanoparticles. Nauka i tehnologii v promyishlennosti. 2011;**1**:90-99

[3] FilippousiM, AngelakerisM, KatsikiniM, PalouraEC, EfthimiopoulosI, WangY, ZamboulisD, Van Tendeloo G. Surfactant effects on the structural and on the magnetic properties of iron oxide nanoparticles. Journal of Physical Chemistry C. 2014;**118**(29):16209-16217. DOI: 10.1021/jp5037266

[4] Uvarova IV, Maksymenko VB. Bio-compatible Materials for Medical Products. Kyiv: KiM; 2013. p. 232

[5] Fang C, Zhang M. Multifunctional magnetic nanoparticles for medical imaging applications. Journal of Materials Chemistry. 2009;**19**:6258-6266. DOI: 10.1039/B902182E

[6] Peng S, Wang C, Xie J, Sun S. Synthesis and stabilization of monodisperse Fe nanoparticles. Journal of the American Chemical Society. 2006;**28**:10676-10677

[7] Gillich T, Acikgöz C, Isa L, Schlüter AD, Spencer ND, Textor M. PEG-stabilized core-shell nanoparticles: Impact of linear versus dendritic polymer shell architecture on colloidal properties and the reversibility of temperature-induced aggregation. ACS Nano. 2013;**7**:316-329

[8] Lalatonne Y, Paris C, Serfaty JM, Weinmann P, Lecouvey M, Motte L. Bis-phosphonates-ultra small superparamagnetic iron oxide nanoparticles: A platform towards diagnosis and therapy. Chemical Communications. 2008;**22**:2553-2555

[9] Hosseini AG, Bagheri M, Mohammad-Rezaei R. Synthesis and fluorescence studies of dual-responsive nanoparticles based on amphiphilic azobenzene-contained poly(monomethyl itaconate). Journal of Polymer Research. 2016;**23**(8):12. DOI: 10.1007/s10965-016-1061-y

[10] Rozenfel'd LH, Chekman IS, Tertyshna AI. Nanotechnology in medicine, pharmacy and pharmacology. Farmakolohiya ta likars'ka toksykolohiya. 2008;**1-3**:3-14

[11] Barrera C, Herrera AP, Bezares N, Fachini E, Olayo-Valles R, Hinestroza JP, Rinaldi C. Effect of poly(ethylene oxide)-silane graft molecular weight on the colloidal properties of iron oxide nanoparticles for biomedical applications. Journal of Colloid and Interface Science. 2012;**377**:40-50

[12] Liu Y, Li Y, Li XM, He T. Kinetics of (3-aminopropyl)triethoxylsilane (APTES) silanization of superparamagnetic iron oxide nanoparticle. Langmuir. 2013;**29**:15275-15282

[13] Sun J, Zhou S, Hou P, Yang Y, Weng J, Li X, Li M. Synthesis and characterization of biocompatible Fe_3O_4 nanoparticles. Journal of Biomedical Materials Research Part A. 2006;**80**(2):333-341

[14] Shu Z, Wang S. Synthesis and characterization of magnetic nanosized Fe_3O_4/MnO_2 composite particles. Journal of Nanomaterials. 2009;**2009**:340217. DOI: 10.1155/2009/340217

[15] Ahangaran F, Hassanzadeh A, Nouri S. Surface modification of Fe_3O_4/SiO_2 microsphere by silane coupling agent. International Nano Letters. 2013;**3**:23

[16] Arsalani N, Fattahi H, Nazarpoor M. Synthesis and characterization of PVP-functionalized superparamagnetic Fe_3O_4 nanoparticles as an MRI contrast agent. eXPRESS Polymer Letters. 2010;**4**(6):329-338

[17] Husain Q. Magnetic nanoparticles as a tool for the immobilization/stabilization of hydrolases and their applications: An overview. Biointerface Research in Applied Chemistry. 2016;**6**(6):1585-1606

[18] Huang HY, Lovell JF. Advanced functional nanomaterials for theranostics. Advanced Functional Materials. 2017;**27**(2):1603524. DOI: 10.1002/adfm.201603524

[19] Pankhurst Q, Connolly J. Applications of magnetic nanoparticles in biomedicine. Journal of Physics D: Applied Physics. 2003;**36**:167-181

[20] Xu C, Sun S. New forms of superparamagnetic nanoparticles for biomedical applications. Advanced Drug Delivery Reviews. 2013;**65**:732-743

[21] Long NV, Thi CM, Yong Y, Cao Y, Wu H, Nogami M. Synthesis and characterization of Fe–based metal and oxide based nanoparticles: Discoveries and research highlights of potential applications in biology and medicine. Recent Patents on Nanotechnology. 2014;**8**:52-61

[22] Huang DJ, Lin H-J, Okamoto J, Chao KS, Jeng H-T, Guo GY, Hsu C-H, Huang C-M, Ling DC, Wu WB, Yang CS, Chen CT. Charge-orbital ordering and Verwey transition in magnetite measured by resonant soft X-ray scattering. Physical Review Letters. 2006;**96**(9):096401. DOI: 10.1103/PhysRevLett.96.096401

[23] Radisavljevic I, Kuzmanovic B, Novakovic N, Mahnke HE, Vulicevic LJ, Kurko S, Ivanovic N. Structural stability and local electronic properties of some EC synthesized magnetite nanopowders. Journal of Alloys and Compounds. 2017;**697**:409-416. DOI: 10.1016/j.jallcom.2016.11.090

[24] Nikiforov VN, Ignatenko AN, Irhin VY. The magnetism of the magnetite nanoparticles: Effects of finite size and coating. Izvestiya RAN. Seriya fizicheskaya. 2014;**78**(10):1336-1340. DOI: 10.7868/S0367676514100159

[25] Duriagina ZA, Holyaka RL, Borysyuk AK. Automated widely diapazon magnetometer for magnetic alloys phase analysis: Development and application. Uspehi Fiziki Metallov; 2013;**14**:33-66

[26] Kondyr AI, Borysyuk AK, Pazdriy IP, Shvachko SH. The use of a vibrating magnetometer for phase analysis of special steels and alloys. Vybratsyy v tekhnyke y tekhnolohyyakh. 2004;**34**(2):41

[27] Koh I, Josephson L. Magnetic nanoparticle sensors. Sensors. 2009;**9**:8130-8145. DOI: 10.3390/s91008130

[28] Janssen XJA, van Ijzendoorn LJ, Prins MWJ. On-chip manipulation and detection of magnetic particles for functional biosensors. Biosensors and Bioelectronics. 2008;**23**:833-838. DOI: 10.1016/j.bios.2007.08.023

[29] Popovic RS. Hall Effect Devices. CAT# IPE331. 2nd ed. Bristol and Philadelphia, USA;CRC Press, 2003. p. 420. ISBN: 9780750308557. Available from: https://www.crcpress.com/Hall-Effect-Devices-Second-Edition/Popovic/p/book/9780750308557

[30] Popovic DR, Dimitrijevic S, Blagojevic M, Kejik P, Schurig E, Popovic RS. Three-axis teslameter with integrated Hall probe. IEEE Transactions on Instrumentations and Measurement. 2007;**56**(4):1396-1402. DOI: 10.1109/TIM.2007.900133

[31] wikipedia.org. Magnetoresistance [Internet]. Available from: https://en.wikipedia.org/wiki/Magnetoresistance

[32] honeywell.com. 3-Axis Digital Compass IC HMC5883L [Internet]. 2010. Available from: https://aerocontent.honeywell.com/aero/common/documents/myaerospacecatalog-documents/Defense_Brochures-documents/HMC5843.pdf

[33] Bolshakova I, Holyaka R. Multiposition 3-D Magnetic Field Sensor [Internet]. European Patent Office, Patent No. WO2005029604. 2005. Available from: https://worldwide.espacenet.com/searchResults?ST=singleline&locale=en_EP&submitted=true&DB=&query=WO2005029604

[34] Bolshakova I, Holyaka R. Method for Measuring Magnetic Field [Internet]. European Patent Office, Patent No. WO2012054000. 2012. Available from: https://worldwide.espacenet.com/searchResults?ST=singleline&locale=en_EP&submitted=true&DB=&query=WO2012054000

[35] Bolshakova I, Holyaka R. Magnetic Field Measuring Sensor [Internet]. European Patent Office, Patent No. WO2006028425. 2006. Available from: https://worldwide.espacenet.com/searchResults?ST=singleline&locale=en_EP&submitted=true&DB=&query=WO2006028425

[36] Bolshakova I, Holyaka R. Magnetic Field Measuring Sensor [Internet]. European Patent Office, Patent No. WO2006028427. 2006. Available from: https://worldwide.espacenet.com/searchResults?ST=singleline&locale=en_EP&submitted=true&DB=&query=WO2006028427

[37] Bolshakova I, Holyaka R. Magnetic Field Measuring Sensor [Internet]. European Patent Office, Patent No. WO2006028426. 2006. Available from: https://worldwide.espacenet.com/searchResults?ST=singleline&locale=en_EP&submitted=true&DB=&query=WO2006028426

[38] Bolshakova I, Holyaka R, Murari A. Method for Measuring Magnetic Field [Internet]. European Patent Office, Patent No. EP2630511. 2015. Available from: https://worldwide.espacenet.com/searchResults?ST=singleline&locale=en_EP&submitted=true&DB=&query=EP2630511

[39] Bolshakova I, Holyaka R, Gerasimov S. Magnetic Field Measurement with Continuous Calibration [Internet]. European Patent Office, Patent No. GB2427700. 2009. Available from: https://worldwide.espacenet.com/searchResults?ST=singleline&locale=en_EP&submitted=true&DB=&query=GB2427700

[40] Hotra Z, Holyaka R, Marusenkova T, Ilkanych V. Algorithms of semiconductor magnetic field sensor devices power consumption minimization. In: ELNANO; 2012; Kyiv. pp. 29-30. Available from: http://journals.kpi.ua/publications/text/29_30_2012.pdf

[41] Hotra Z, Holyaka R, Marusenkova T. Optimization of microelectronic magnetic sensors on the splitted Hall structures. In: Prace Instytutu Elektrotechniki, editor. Proceedings of Electrotechnical Institute, Instytut Elektrotechniki. Issue 247. 2010. pp. 13-18. Available from: https://pbn.nauka.gov.pl/polindex-webapp/browse/article/article-4d222aa0-9679-45e1-9467-5c5de8b262f6

[42] Hotra Z, Holyaka R, Bolshakova I, Yurchak I, Marusenkova T. Spatial models of splitted Hall structures. In: Proceedings of VIIth International Conferenceon Perspective Technologies and Methods in MEMS Design; MEMSTECH–2011; IEEE.2011. pp. 5-8. Available from: http://ieeexplore.ieee.org/document/5960249/

[43] Holyaka R, Yurchak I, Marusenkova T, Ilkanych V. Microprocessor noise-immune signal transducer for galvanomagnetic smart sensor devices. In: International Conferenceon Modern Problems of Radio Engineering Telecommunications and Computer Science; TCSET–2012; IEEE.2012. p. 430. Available from: http://ieeexplore.ieee.org/document/6192682/

[44] Bolshakova I, Holyaka R, Hotra Z, Marusenkova T. Methods of modeling and calibrating 3D magnetic sensors based on splitted Hall structures. Electronics and Nanotechnologies. Proceedings of the XXXI International Scientific Conference. 2011; p. 38. Available from: http://www.journals.kpi.ua/publications/text/2011_38.pdf

IntechOpen